Original Paper

phys. stat. sol. (a) **204**, No. 2, 439–446 (2007) / **DOI** 10.1002/pssa.200673963

Electronic band structure of wurtzite InN around the fundamental gap in the presence of biaxial strain

Jayeeta Bhattacharyya and **Sandip Ghosh***

Department of Condensed Matter Physics and Material Science, Tata Institute of Fundamental Research, Homi Bhabha Road, Mumbai 400005, India

Received 18 September 2006, revised 26 October 2006, accepted 24 October 2006
Published online 6 February 2007

PACS 71.20.Nr, 78.20.Bh, 78.66.Fd

We present results of a theoretical study of the electronic band structure of wurtzite InN films under biaxial strain in the *C*-plane (0001) and in planes that correspond to non-polar orientations such as the *A*-plane $(11\bar{2}0)$ and the *M*-plane $(1\bar{1}00)$. The calculations are performed under the $\boldsymbol{k}\cdot\boldsymbol{p}$ perturbation theory approach using the Bir–Pikus Hamiltonian. The results show that the fundamental bandgap of InN shifts by 30 meV (14 meV) for isotropic tensile (compressive) strain in the *C*-plane with out-of-plane contraction (dilation) of 0.2%. For films of non-polar orientations, the *c*-axis lies in the film plane and the strain is expected to be different between directions parallel and perpendicular to *c*. Such anisotropic strain give rise to valence band mixing which results in dramatic changes in the optical polarization properties as evidenced by the calculated oscillator strengths of the interband transitions.

1 Introduction

III–V wurtzite nitrides and their alloys are today amongst the most intensely investigated semiconductors for light emitting device and lasers applications. However the electronic band structure (EBS) of one member, namely InN, continues to be a subject of debate. In the recent past, studies [1, 2] have suggested the value of the bandgap to be close to 0.7 eV at 10 K, much lower than the previously accepted value of 1.9 eV. Thereafter, there have been reports favoring either of the two values [3]. Those supporting a high value for the bandgap suggest that the observed low energy photoluminescence (PL) and absorption signals arise from deep traps [4, 5], Mie scattering [6] or non-stoichiometry [7]. Advocates for a lower value for the bandgap suggest that the observations indicating higher bandgap originate from oxygen contamination [8] and doping related Moss–Burstein shift [9]. Due to large lattice constant mismatch of InN ($a = 3.5376$ Å, $c = 5.7064$ Å) with respect to substrates such as sapphire ($a = 4.7564$ Å, $c = 12.989$ Å), the InN films are probably relaxed at the growth temperature, but a strain invariably develops in the film due to the mismatch in thermal-expansion coefficients between the film and the substrate, as the film cools down. Such in-plane strain can also shift the bandgap although by relatively smaller amounts, but this needs to be determined for accurate estimate of the bandgap and is the main motivation of this work.

Modulation spectroscopy techniques such as Photo-reflectance and Electro-reflectance provide the most reliable estimates of the critical point energies in the EBS. However currently most estimates of the bandgap of InN have been based on PL and absorption studies, because the presence of surface charges prevent efficient electro-modulation [10]. With improvements in material quality it should be possible to perform such measurements in future. The other motivation of this work is to predict the polarization

* Corresponding author: e-mail: sangho10@tifr.res.in, Phone: +91-22-22782840, Fax: +91-22-22804610

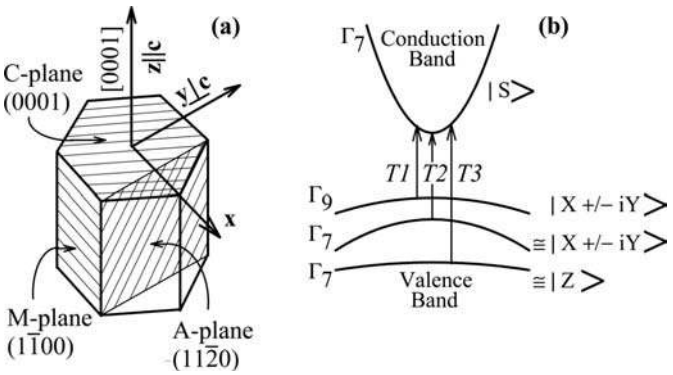

Fig. 1 (a) Wurtzite unit cell of InN showing the *C*-plane, the *A*-plane, and the *M*-plane and the choice of coordinates. (b) Schematic of the electronic band structure of InN around the fundamental gap in the absence of strain.

characteristics and energy shifts of the interband transitions in InN under biaxial strain for the analysis of modulation spectroscopy data.

Currently most nitride heterostructure light emitting devices are based on [0001] oriented *C*-plane films [see Fig. 1(a)] with the polar *c*-axis normal to the film. These however suffer from loss of radiative efficiency due to large piezo- and pyro-electric fields along the polar axis. This can be avoided by growing devices with films of non-polar orientation where the *c*-axis lies in the film plane such as the *A*-plane (11$\bar{2}$0) and the *M*-plane (1$\bar{1}$00) [11]. In this study we have therefore considered the effect of biaxial strain not just in the *C*-plane but also the *A*-plane and the *M*-plane. We first describe the calculation procedure and the parameters used and then go on to the results and discuss their implications.

2 Electronic band structure calculations

As in the case of GaN, around the fundamental gap of unstrained wurtzite InN at the Brillouin zone center (wave vector $\boldsymbol{k} = 0$), there is one conduction band (CB) Γ_7 and three closely spaced valence bands (VB) Γ_9, Γ_7^{upper}, and Γ_7^{lower} [see Fig. 1(b)]. The bands have spin degeneracy factor of 2. The *c*-axis defines the *z*-direction. To theoretically estimate the strain induced modification of these bands, we adopt the $\boldsymbol{k} \cdot \boldsymbol{p}$ perturbation approach outlined by Bir and Pikus [12]. For a narrow bandgap (E_g) semiconductor one should consider interactions between the VB and the CB which needs a full 8×8 band calculation. This Hamiltonian has the form

$$H(\boldsymbol{k}) = \begin{bmatrix} H_{cc} & H_{cv} \\ H_{cv}^{\dagger} & H_{vv} \end{bmatrix}.$$

Here H_{cc} is a 2×2 matrix for the CB and H_{vv} is a 6×6 matrix for the VB without any interaction between them and are given by

$$H_{cc} = \begin{bmatrix} E^c & 0 \\ 0 & E^c \end{bmatrix}, \qquad H_{vv} = \begin{bmatrix} F & 0 & -H^* & 0 & K^* & 0 \\ 0 & G & \Delta & -H^* & 0 & K^* \\ -H & \Delta & \lambda & 0 & I^* & 0 \\ 0 & -H & 0 & \lambda & \Delta & I^* \\ K & 0 & I & \Delta & G & 0 \\ 0 & K & 0 & I & 0 & F \end{bmatrix},$$

where

$$F = \Delta_1 + \Delta_2 + \lambda + \theta\,, \qquad G = \Delta_1 - \Delta_2 + \lambda + \theta\,, \qquad H = i(A_6 k_z k_+ + A_7 k_+ + D_6 \varepsilon_{z+})\,,$$

$$I = i(A_6 k_z k_+ - A_7 k_+ + D_6 \varepsilon_{z+})\,, \qquad K = A_5 k_+^2 + D_5 \varepsilon_+\,, \qquad \Delta = \sqrt{2}\Delta_3\,,$$

$$\lambda = A_1 k_z^2 + A_2 k_\perp^2 + D_1 \varepsilon_{zz} + D_2(\varepsilon_{xx} + \varepsilon_{yy})\,, \qquad \theta = A_3 k_z^2 + A_4 k_\perp^2 + D_3 \varepsilon_{zz} + D_4(\varepsilon_{xx} + \varepsilon_{yy})\,,$$

$$\varepsilon_+ = \varepsilon_{xx} - \varepsilon_{yy} + 2i\varepsilon_{xy}\,, \qquad \varepsilon_{z+} = \varepsilon_{xz} + i\varepsilon_{yz}\,, \qquad k_+ = k_x + ik_y\,, \qquad k_\perp^2 = k_x^2 + k_y^2\,. \tag{1}$$

The parameters D_j ($j = 1$ to 6) denote the deformation potentials for the VB, A_j ($j = 1$ to 7) are equivalent to the Luttinger parameters and determine the hole effective masses. $\varepsilon_{l,m}$ and k_l ($l, m = x, y, z$) are the strain tensor and wave vector components, respectively. Δ_1 and Δ_2 are the crystal field and spin–orbit energy splitting parameters, respectively. The basis functions at $\boldsymbol{k} = 0$ were $\left(1/\sqrt{2}\right)|X + iY, \alpha\rangle$, $\left(1/\sqrt{2}\right)|X + iY, \beta\rangle$, $|Z, \alpha\rangle$, $|Z, \beta\rangle$, $\left(1/\sqrt{2}\right)|X - iY, \alpha\rangle$, $\left(1/\sqrt{2}\right)|X - iY, \beta\rangle$ for the VB and $|S, \alpha\rangle$ and $|S, \beta\rangle$ for the CB. Here the Bloch functions $|S\rangle$, $|X\rangle$, $|Y\rangle$, and $|Z\rangle$ have symmetry properties of the atomic s, p_x, p_y, and p_z orbital functions. $|\alpha\rangle$ and $|\beta\rangle$ denote the spin wave functions corresponding to spin up and spin down. The CB-VB interaction is treated as a second-order perturbation and is given by the following 2×6 matrix

$$H_{\mathrm{cv}} = \begin{bmatrix} Q & 0 & R & 0 & Q^* & 0 \\ 0 & Q & 0 & R & 0 & Q^* \end{bmatrix},$$

where $Q = \left(\hbar/\sqrt{2}m_0\right)\langle S|\, p_x|X\rangle\, k_+$ and $R = (\hbar/m_0)\,\langle S|\, p_z|Z\rangle\, k_z$ with p_x and p_z representing momentum operators. Since the interaction matrix components vanish at $\boldsymbol{k} = 0$, we can separately consider CB and the VB Hamiltonians. Diagonalisation of the latter yields three distinct VB energies $E_n^{\mathrm{v}}(\boldsymbol{k} = 0)$. The single eigenvalue for the CB minimum can be expressed as [13]

$$E^{\mathrm{c}}(\boldsymbol{k}) = E^{\mathrm{c}}(\boldsymbol{k} = 0) + \frac{\hbar^2 k_z^2}{2m_{\parallel}^{\mathrm{e}}} + \frac{\hbar^2(k_x^2 + k_y^2)}{2m_{\perp}^{\mathrm{e}}}, \qquad E^{\mathrm{c}}(\boldsymbol{k} = 0) = \alpha_{\parallel}\varepsilon_{zz} + \alpha_{\perp}(\varepsilon_{xx} + \varepsilon_{yy})\,, \tag{2}$$

where $\alpha_{\parallel,\perp}$ and $m_{\parallel,\perp}^{\mathrm{e}}$ denote the CB deformation potential and the electron effective mass parallel ($\parallel$) and perpendicular ($\perp$) to the c-axis. The excitonic transition energies may then be approximated as

$$E_n\,(\boldsymbol{k} = 0) = E^* + E^{\mathrm{c}}(\boldsymbol{k} = 0) - E_n^{\mathrm{v}}(\boldsymbol{k} = 0) - E_{\mathrm{ex}}^{\mathrm{b}}\,, \tag{3}$$

where $E_{\mathrm{ex}}^{\mathrm{b}}$ is the exciton binding energy considered same for all three transitions here, $E^* = E_{\mathrm{g}} + \Delta_1 + \Delta_2$ where E_{g} is chosen to match the experimental ground state transition energy. The components of the oscillator strengths for the transitions, which determine the polarization selection rules, are obtained from momentum matrix elements of the type $|\langle \Psi^{\mathrm{CB}}|\, p_l\, |\Psi^{\mathrm{VB}}\rangle_n|^2$ with $l = x, y, z$. Here $\langle \Psi^{\mathrm{CB}}| = \langle S, \alpha|$ and $\langle S, \beta|$, while $|\Psi^{\mathrm{VB}}\rangle_n = \sum_{i=1}^{6} a_{ni}[i^{\mathrm{th}}$ VB basis function$]$. The coefficients a_{ni} are obtained by determining the eigenvectors of H_{vv}. The relative values of $|\langle S|\, p_x|X\rangle|^2$, $|\langle S|\, p_y|Y\rangle|^2$, and $|\langle S|\, p_z|Z\rangle|^2$ are known to be equal in GaN. In InN too, under quasi cubic approximation, their values are nearly equal, the difference being ~ 2% [13].

The relation between the in-plane and the out-of-plane strain components, which are needed for the calculations, can be obtained as follows. An A-plane film under in-plane biaxial strain is free to expand or contract in the out-of-plane direction. This implies that the out-of-plane stress component $\sigma_{xx} = 0$ and leads to the following relation between the strain components

$$\varepsilon_{xx} = -\frac{C_{12}}{C_{11}}\varepsilon_{yy} - \frac{C_{13}}{C_{11}}\varepsilon_{zz}, \qquad \varepsilon_{xy} = \varepsilon_{yz} = \varepsilon_{zx} = 0\,, \tag{4}$$

where C_{ij} are the elastic stiffness constants. Due to the symmetry of the system the effect of strain in the *y*-*z*-plane is identical to the case of strain in the *x*-*z*-plane and so for the case of *M*-plane strain we can interchange *x* and *y* to arrive at the required result. For the *C*-plane case we have

$$\varepsilon_{zz} = -\frac{C_{13}}{C_{33}}\varepsilon_{xx} - \frac{C_{13}}{C_{33}}\varepsilon_{yy}, \qquad \varepsilon_{xy} = \varepsilon_{yz} = \varepsilon_{zx} = 0\,. \tag{5}$$

Thus to specify isotropic strain in the *C*-plane ($\varepsilon_{xx} = \varepsilon_{yy}$) we need only one strain parameter (ε_{zz}) but for *A*-plane and *M*-plane cases where the strain may not be isotropic we need two strain parameters, ($\varepsilon_{yy}, \varepsilon_{zz}$) and ($\varepsilon_{xx}, \varepsilon_{zz}$) respectively.

For calculations at $\boldsymbol{k} = 0$, the number of required parameters ($\alpha_{\|}$, $\alpha_{\perp}$, D_1 to D_5, Δ_i) is smaller. The local atomic coordination of a wurtzite structure is the same as that for a cubic zincblende structure and differs only for the relative positions of the third nearest neighbors and beyond. This justifies a quasi-cubic approximation [12] which relates some of the parameters as follows

$$\alpha_{\|} = \alpha_{\perp} = \alpha\,, \qquad D_3 = D_2 - D_1\,, \qquad 2D_4 = -D_3\,, \qquad \Delta_3 = \Delta_2\,. \tag{6}$$

The remaining deformation potentials [14] required were $\alpha = -7.2$ eV, $D_1 = -3.7$ eV, $D_2 = 4.5$ eV, $D_5 = -4.0$ eV, and splittings $\Delta_1 = 19$ meV, $\Delta_2 = 1.7$ meV [15]. The elastic constants were $C_{11} = 223$ GPa, $C_{12} = 115$ GPa, $C_{13} = 92$ GPa, $C_{33} = 224$ GPa [14].

3 Results and discussions

The actual bandgap of InN is still a subject of debate and since we are mainly interested in transition energy shifts due to strain, we therefore present our results in terms of energy shifts relative to the *low temperature* bandgap of unstrained InN taken to be 0.7 eV here. A *C*-plane InN sample is typically grown on *C*-plane sapphire or *C*-plane 6H-SiC and in such cases the in-plane strain is isotropic whereby $\varepsilon_{xx} = \varepsilon_{yy}$. Due to strain the VBs can cross each other and get mixed, so for practical labeling of the transitions we adopt a nomenclature, identical to that suggested for GaN [16], of the type $T1$, $T2$ and $T3$ in the order of increasing transition energy $E_1 < E_2 < E_3$ for a given strain condition. Figure 2 shows the calculated energy shift of these three transitions around the fundamental gap of InN due to isotropic *C*-plane strain and Fig. 3 shows their oscillator strengths $f_{i\beta}$ ($i \to T1, T2, T3$ and $\beta \to x, y, z$) for the three polarizations along *x*-, *y*- and *z*-directions.

These results show that for unstrained InN the wavefunction (at $\boldsymbol{k} = 0$) of the top VB has $|X\rangle$, $|Y\rangle$ type symmetry, the next one has predominantly $|X\rangle$, $|Y\rangle$ type symmetry and the bottom one has mainly $|Z\rangle$

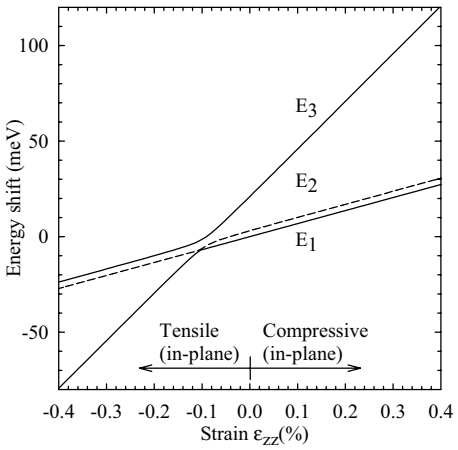

Fig. 2 Variation in the energy E_1, E_2 and E_3 of the transitions $T1$, $T2$ and $T3$ of InN for isotropic *C*-plane strain, defined by ε_{zz}, relative to the value of E_1 in the absence of strain. $T1$ ($T3$) is defined as the transition with the lowest (highest) transition energy for a given strain value.

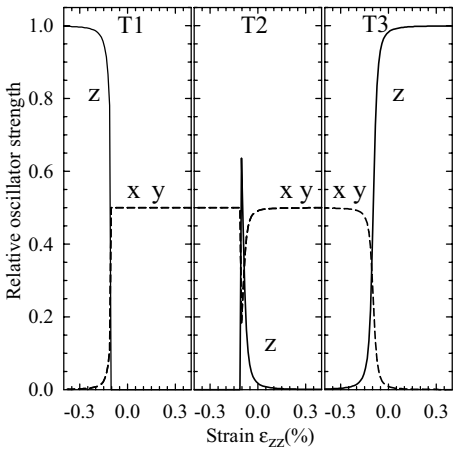

Fig. 3 Relative oscillator strengths $f_{i\beta}$ ($i = 1, 2, 3$ and $\beta = x, y, z$) of the three transitions $T1$, $T2$, and $T3$ of InN for x (dashed line), y (dashed line), z (continuous line) polarization as a function of isotropic C-plane strain defined by ε_{zz}. x- and y-polarization results are identical.

type symmetry just as was indicated in Fig. 1(b). With strain these symmetries change as the VB mix and move. Thus for in-plane tensile strain with $\varepsilon_{zz} < -0.1\%$ we see that the lowest energy transition $T1$ is predominantly z-polarized while it is mostly x- and y-polarized for compressive in-plane strain. Again for compressive strain $T3$ is mostly z-polarized. These oscillator strength values obey the following two sum rules $f_{ix} + f_{iy} + f_{iz} = 1$ and $f_{1\beta} + f_{2\beta} + f_{3\beta} = 1$. Since it is difficult to probe a C-plane film with light of z-polarization, in an unstrained or compressively strained C-plane InN film it would be difficult to observe the third transition $T3$. Similarly for tensile strain with $\varepsilon_{zz} < -0.1\%$ it would be difficult to observe the $T1$ transition which defines the effective bandgap. Notice also that there is no difference between the oscillator strengths for x- and y-polarization, therefore for isotropic C-plane strain there is no in-plane optical polarization anisotropy. Figure 2 shows that for compressive in-plane strain with $\varepsilon_{zz} = 0.2\%$, which is within the range of strain values one can expect, the energy of transition $T1$ blue shifts by 14 meV. For in-plane tensile strain with $\varepsilon_{zz} = -0.2\%$ there is a red shift of $T1$ by 30 meV. For comparison these numbers for GaN, with C-plane strain of similar magnitude, are 31 meV and 54 meV for in-plane compressive and tensile strain respectively [17]. Thus these shifts in the bandgap energy with strain are quite small compared to the magnitude of discrepancy in the bandgap of InN as measured by various groups [3] and obviously cannot account for it. However these shifts would be clearly measurable in a modulation spectroscopy measurement on good quality InN samples.

We next discuss the case of A-plane films where the c-axis lies in the film plane. In an unstrained A-plane InN film one can therefore expect to see all the three interband transitions since measurements with both light electric field $E \perp c$ and $E \| c$ can be easily performed on such a sample. Such films however are typically grown on R-plane sapphire ($1\bar{1}02$) [18] and are likely to be strained due to thermal expansion coefficient mismatch with the substrate. Moreover since the thermal expansion coefficient of InN is different between the directions $\| c$ (2.9×10^{-6} K^{-1}) and $\perp c$ (3.8×10^{-6} K^{-1}), this strain is likely to be anisotropic whereby $\varepsilon_{yy} \neq \varepsilon_{zz}$. In Fig. 4 the first contour plot shows the variation of the out-of-plane strain ε_{xx} as a function of in-plane strain coordinates ($\varepsilon_{yy}, \varepsilon_{zz}$). It shows how a value of ε_{xx}, which may be determined through a high resolution X-ray diffraction measurement, corresponds to a range of in-plane strain values. Therefore one needs at least two out of the three strain parameters ε_{xx}, ε_{yy} and ε_{zz}, to determine the band structure modifications and we have performed calculations for a general in-plane strain coordinate ($\varepsilon_{yy}, \varepsilon_{zz}$). The other three contour plots in Fig. 4 show the shift in the three transition energies relative to the unstrained value of E_1 as a function of in-plane strain ($\varepsilon_{yy}, \varepsilon_{zz}$) in the A-plane. We find that the magnitude of the energy shifts are similar to those for strain in the C-plane.

The plots in Fig. 5 show the calculated oscillator strength components of the three interband transitions as a function in-plane strain in the A-plane. To bring out the essence of these plots we take two cases. First consider an overall in-plane tensile strain situation defined by coordinates ($\varepsilon_{yy} = 0.1\%, \varepsilon_{zz} = 0.2\%$)

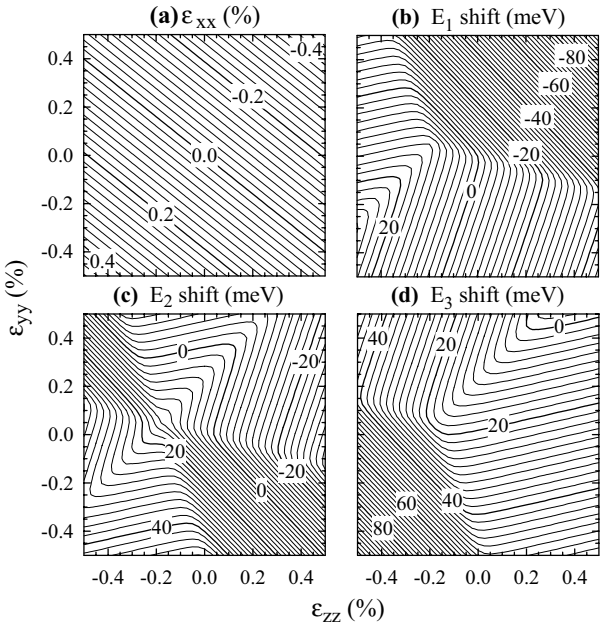

Fig. 4 Contour plots showing the variation in the out-of-plane strain ε_{xx} with in-plane strain ε_{yy} and ε_{zz} in the A-plane. (b) Shift in the energy E_1 of the transition $T1$ of InN with A-plane strain relative to the unstrained value of E_1. (c) Shift in energy E_2 of the transition $T2$, relative to unstrained E_1 value. (d) Shift in energy E_3 of the transition $T3$, relative to unstrained E_1 value. $T1$ ($T3$) is defined as the transition with the lowest (highest) transition energy for a given in-plane strain value.

and marked by the squares in the plots of Fig. 5. We see that the y- and z-components of the oscillator strength for $T1$ is relatively negligible in value as compared to the x-component. Since luminescence is expected to be dominated by the lowest energy transition $T1$ due to excess carrier population statistics, this means that such a sample will show poor out of plane emission. In a modulation spectroscopy experiment on such a sample one would most likely see only the transitions $T2$ (for $E \perp c$) and $T3$ (for $E \| c$) and therefore one must be careful in identifying these transitions. Such phenomenon has in fact been observed through absorption measurements [19], however it was difficult to get an accurate estimate of the transition energies due to the presence of sub-bandgap absorption tails, modulation spectroscopy measurements on better quality samples can prove useful here. Next consider a case of overall in-plane compressive strain defined by coordinates ($\varepsilon_{yy} = -0.3\%$, $\varepsilon_{zz} = -0.2\%$) and marked by the circles in the plots of Fig. 5. Here we see that the y-polarized component of $T1$ and z-polarized component of $T2$ are very strong while the third transition $T3$ is predominantly x-polarized. This corresponds to an effective polarization dependent optical bandgap change. Thus in an experiment on such a sample we expect to see $T1$ for $E \perp c$ and $T2$ for $E \| c$ and may not see $T3$ at all. We therefore see that in strained A-plane films there is strong in-plane optical polarization anisotropy. The transition energy shifts and oscillator strengths for biaxial strain in the M-plane would be identical to that in the A-plane case for the same values of in-plane strain ($\| c$ and $\perp c$) and light polarization relative to the c-axis. Therefore if we interchange x and y everywhere in Fig. 5 we will get the results for strain in the M-plane.

A wurtzite crystal is inherently expected to show anisotropy in its optical properties between light polarized with $E \| c$ and $E \perp c$ from symmetry considerations. What we have shown here is that with anisotropic strain in the A-plane and the M-plane of InN, the optical polarization anisotropy can be significantly enhanced with some transitions not being seen at all for certain polarizations of the probe light. In the case of C-plane films such in-plane optical polarization anisotropy does not arise for isotropic

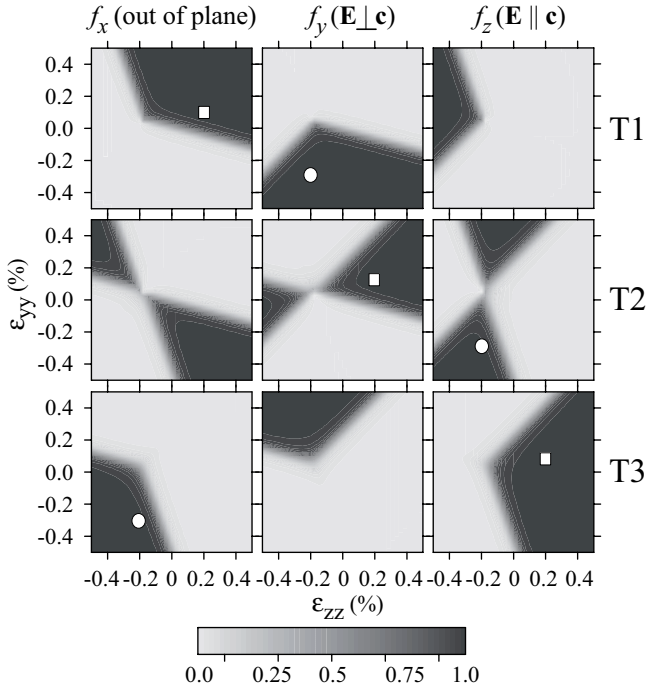

Fig. 5 Relative magnitudes $f_{i\beta}$ ($i = 1, 2, 3$ and $\beta = x, y, z$) representing the oscillator strengths for the three transitions $T1$, $T2$, and $T3$ of InN as a function of in-plane strain ε_{yy} and ε_{zz} in the A-plane. The circles mark the in-plane strain coordinates ($\varepsilon_{yy} = -0.3\%$, $\varepsilon_{zz} = -0.2\%$) and the squares mark ($\varepsilon_{yy} = 0.1\%$, $\varepsilon_{zz} = 0.2\%$). For the case of strain in the M-plane, the results are the same as here if x and y are interchanged everywhere.

strain, however there too if the strain is anisotropic and distorts the symmetry of the crystal in the plane perpendicular to the c-axis, an in-plane anisotropy may arise [20], but in most C-plane InN film growth situations such anisotropic strain do not occur. The magnitudes of the deformation potentials and the energy splitting parameters affect the polarization properties [21] and their precise values for InN is still not a settled issue, however the overall nature of the polarization characteristics as described above will not change.

The strain dependence of the interband transitions in InN around the fundamental gap as described here is similar to that for GaN [16, 22], the difference arises mainly in terms of the magnitude of the energy shifts. Thus it follows that in nitride optoelectronic devices with large In concentration in the active region in the form of $In_xGa_{1-x}N$, in-plane strain will play an important role in determining device performance. For instance if edge-emitting lasers are made using A-plane oriented structures, efficient lasing in the transverse electric mode can occur for compressive in-plane strain but it would be necessary to orient the laser cavity along the c-axis, since light with $E \| y$ will not travel along y-direction. Such films with high in-plane compressive strain can also used for polarization sensitive photo-detector applications [23, 24]. For vertical cavity surface emitting laser applications in-plane tensile strain should be avoided since for such strain the emission will be polarized normal to the growth plane which is also the cavity direction.

4 Conclusions

In conclusion we have presented results that show how the electronic band structure around the fundamental gap of wurtzite InN films are modified by in-plane biaxial strain. For C-plane films under iso-

tropic strain the bandgap shifts but there is no in-plane polarization anisotropy. For *A*-plane and *M*-plane films the bandgap shift is accompanied by strong in-plane polarization anisotropy and this will have to be taken into account for analyzing experimental data as well as in optoelectronic device designs.

Acknowledgements The authors would like to thank B. M. Arora, H. T. Grahn, W. J. Schaff, O. Brandt, and A. Bhattacharya for many useful discussions at different times.

References

[1] V. Y. Davydov, A. A. Klochikhin, R. P. Seisyan, V. V. Emtsev, S. V. Ivanov, F. Bechstedt, J. Furthmüller, H. Harima, A. V. Mudryi, J. Aderhold, O. Semchinova, and J. Graul, phys. stat. sol. (b) **229**, R1 (2002).
[2] J. Wu, W. Walukiewicz, K. M. Yu, J. W. Ager, E. E. Haller, H. Lu, W. J. Schaff, Y. Saito, and Y. Nanishi, Appl. Phys. Lett. **80**, 3967 (2002).
[3] B. Monemar, P. P. Paskov, and A. Kasic, Superlattices Microstruct. **38**, 38 (2005).
[4] K. S. A. Butcher, M. Wintrebert-Fouquet, P. P. T. Chen, H. Timmers, and S. K. Shreshta, Mater. Sci. Semicond. Process. **6**, 351 (2003).
[5] Q. X. Guo, T. Tanaka, M. Nishio, H. Ogawa, X. D. Pu, and W. Z. Shen, Appl. Phys. Lett. **86**, 231913 (2005).
[6] T. V. Shubina, S. V. Ivanov, V. N. Jmerik, D. D. Solnyshkov, V. A. Vekshin, P. S. Kop'ev, A. Vasson, J. Leymarie, A. Kavokin, H. Amano, K. Shimono, A. Kasic, and B. Monemar, Phys. Rev. Lett. **92**, 117407 (2004).
[7] K. S. A. Butcher, M. Wintrebert-Fouquet, P. P. T. Chen, K. E. Prince, H. Timmers, S. K. Shreshta, T. V. Shubina, S. V. Ivanov, R. Wuhrer, M. R. Phillips, and B. Monemar, phys. stat. sol. (c) **2**, 2263 (2005).
[8] A. G. Bhuiyan, K. Sugita, K. Kasashima, A. Hashimoto, A. Yamamoto, and V. Y. Davydov, Appl. Phys. Lett. **83**, 4788 (2003).
[9] J. Wu, W. Walukiewicz, S. X. Li, R. Armitage, J. C. Ho, E. R. Weber, E. E. Haller, H. Lu, and W. J. Schaff, A. Barcz, and R. Jakiela, Appl. Phys. Lett. **84**, 2805 (2004).
[10] H. Lu, W. J. Schaff, L. F. Eastman, and C. E. Stutz, Appl. Phys. Lett. **82**, 1736 (2003).
[11] P. Waltereit, O. Brandt, A. Trampert, H. T. Grahn, J. Menniger, M. Ramsteiner, M. Reiche, and K. H. Ploog, Nature (London) **406**, 865 (2000).
[12] G. L. Bir and G. E. Pikus, Symmetry and Strain Induced Effects in Semiconductors (Wiley, New York, 1974).
[13] M. Suzuki and T. Uenoyama, in: Group III Nitride Semiconductor Compounds, edited by B. Gil (Clarendon, Oxford, 1998).
[14] I. Vurgaftman and J. R. Meyer, J. Appl. Phys. **94**, 3675 (2003).
[15] P. Carrier and S. H. Wei, J. Appl. Phys. **97**, 033703 (2005).
[16] S. Ghosh, P. Waltereit, O. Brandt, H. T. Grahn, and K. H. Ploog, Phys. Rev. B **65**, 75202 (2002).
[17] A. Shikanai, T. Azuhata, T. Sota, S. Chichibu, A. Kuramata, K. Horino, and S. Nakamura, J. Appl. Phys. **81**, 417 (1997).
[18] H. Lu, W. J. Schaff, L. F. Eastman, J. Wu, W. Walukiewicz, V. Cimalla, and O. Ambacher, Appl. Phys. Lett. **83**, 1136 (2003).
[19] Jayeeta Bhattacharyya, S. Ghosh, M. R. Gokhale, B. M. Arora, H. Lu, and W. J. Schaff, Appl. Phys. Lett. **89**, 151910 (2006).
[20] S. Ghosh, P. Waltereit, A. Thamm, O. Brandt, H. T. Grahn, and K. H. Ploog, phys. stat. sol. (a) **192**, 72 (2002).
[21] R. Goldhahn, P. Schley, A. T. Winzer, M. Rakel, C. Cobet, N. Esser, H. Lu, and W. J. Schaff, J. Cryst. Growth **288**, 273 (2006).
[22] S. Ghosh, P. Misra, H. T. Grahn, B. Imer, S. Nakamura, S. P. DenBaars, and J. S. Speck, J. Appl. Phys. **98**, 026105 (2005).
[23] S. Ghosh, O. Brandt, H. T. Grahn, and K. H. Ploog, Appl. Phys. Lett. **81**, 3380 (2002).
[24] C. Rivera, J. L. Pau, E. Muñoz, P. Misra, O. Brandt, H. T. Grahn, and K. H. Ploog, Appl. Phys. Lett. **88**, 213507 (2006).

